Merocyanine Dye-Sensitization of Polythiophene in a Conjugated Polymer/TiO$_2$ p–n Hetero-Junction Solar Cell

Kiyoaki Imoto, Kohshin Takahashi,[*,†] **Takahiro Yamaguchi,**[†] **Teruhisa Komura,**[†]
Jun-ichi Nakamura,[††,#] **and Kazuhiko Murata**[††]

Division of Innovative Technology and Science, Graduate School of Natural Science and Technology,
Kanazawa University, Kodatsuno, Kanazawa 920-8667

†Department of Chemistry and Chemical Engineering, Faculty of Engineering, Kanazawa University,
Kodatsuno, Kanazawa 920-8667

††Performance Chemicals and Materials Research Center, Nippon Shokubai Co., Ltd.,
5-8, Nishi Otabi-cho, Suita, Osaka, 564-8512

Received May 1, 2003; E-mail: ktakaha@t.kanazawa-u.ac.jp

In the blended solid of merocyanine (MC) and polythiophene (PTh)/TiO$_2$ p–n hetero-junction solar cells, a hole-transfer from the excited state of MC to the ground-state of PTh accelerated the charge separation in the depletion layer formed at the TiO$_2$/MC+PTh interface, enhancing the photovoltaic properties. That is, the blended solar cell is not a so-called Grätzel cell being sensitized by mono-layer dyes chemically adsorbed on the TiO$_2$ electrode, but rather the enhanced photovoltaic properties are attributable to the dye-sensitization of the conjugated polymer.

Although organic solar cells have been expected to provide low-cost energy-conversion devices, practical use of them has not been achieved. Tang attained an energy conversion efficiency up to 1% by using a phtalocyanine/perylene derivative p–n junction cell.[1] Recently, conjugated polymer photovoltaics have been extensively studied. For example, Friend et al. attained an energy conversion efficiency up to 1.9% by a poly-[5-(2-ethylhexyloxy)-1,4-phenylenvinylene]/polythiophene double-layer solar cell using soluble conjugated polymers under AM1.5 illumination,[2] Sariciftci et al. attained an energy conversion efficiency up to 3.3% in a p–n hetero-bulk-junction solar cell consisting of a soluble poly[5-(3,7-dimethyloctyl-oxy)-1,4-phenylenvinylene]and a soluble fullerene 60 derivative.[3]

We have examined the performance of organic solar cells with blended solid films of conjugated polymers as a charge-transporting material and dyes as light-harvesting compounds. We have reported that an enhanced photocurrent was observed for an Al/organic solid Schottky-barrier cell with a blended solid film of regioregular polythiophene and a dye such as a porphyrin or a merocyanine.[4–8] However in the cell, the aluminum electrode was photocorroded under illumination.[9]

Recently, p–n heterojunction solar cells composed of an inorganic semiconductor as an electron-transporting material and a conjugated polymer as a light-harvesting and hole-transporting compound have been studied.[10–15] For example, Savenji et al. studied a solar cell consisting of a dense TiO$_2$ thin film and poly[2-methoxy-5-(2′-ethyl-hexyloxy)-1,4-phenylene vinyl-ene] MEH-PPV,[10] Alevilsatos et al. studied a cell consisting of CdSe nano-rods and poly(3-hexylthiophene),[11] and Carter et al. reported on a cell consisting of TiO$_2$ nano-particles and poly[2-methoxy-5-(3′,7′-dimethyl-octyloxy)-1,4-phenylene vinylene] MDMO-PPV.[12] These types of solar cells were photo-stable, but the energy conversion efficiency was low due to the low light-harvesting ability of the conjugated polymer films.

We believe that combining both a blended solid and an inorganic semiconductor promises further improvement in solar cell performance. In this paper, we report an improvement in the photovoltaic properties of a TiO$_2$/regioregular poly(3-hexylthiophene-2,5-diyl)/Au sandwich-type solar cell sensitized with a merocyanine dye.

Experimental

Chemicals. Regioregular poly(3-hexylthiophene-2,5-diyl) (PTh, average molecular weight of ca. 87000) was purchased from Aldrich Chemicals and used without further purification. Mero-cyanine dyes MC1 and MC2 were purchased from Hayashibara Seibutsu Kagaku Lab. and used without further purification. The employed organic compounds and their abbreviations are shown in Fig. 1.

Preparation and Characteristics of TiO$_2$ Electrode. Transparent TiO$_2$ electrodes were prepared as follows: 0.5 mL of distilled water was added to 30 mL of anhydrous ethanol (Kanto Kagaku Co. Ltd.,) and adjusted to pH 1 with concentrated HNO$_3$. 4.26 g of titanium(IV) isopropoxide (Kanto Kagaku Co. Ltd.,) was added to this solution at room temperature under agitation. The solution was stirred at 40 °C for 16 h. This TiO$_2$ sol solution was then spin-coated on an SnO$_2$:F substrate (Nippon Sheet Glass Co. Ltd., <10 Ω/□) at 2000 rpm. The sample was dried at 100 °C for 1 h, then annealed at 450 °C for 1 h. The process from the spin-coating to the annealing was repeated twice.

Division of Innovative Technology and Science, Graduate School of Natural Science and Technology, Kanazawa University
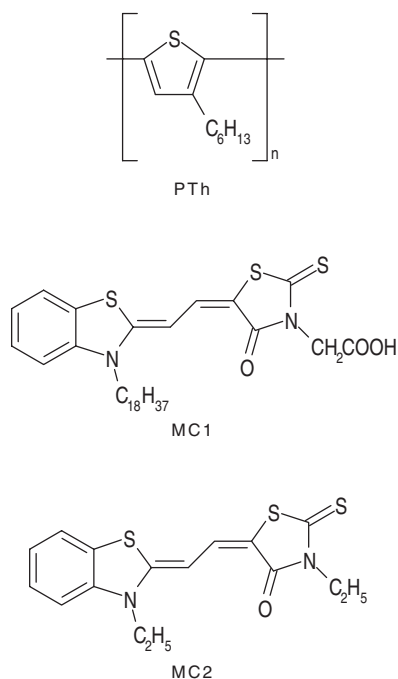
PTh

MC1

MC2

Fig. 1.　Structures of polythiophene and merocyanine dyes.

Cyclic voltammetry was carried out in an N_2 purged acetonitrile solution containing 1 mM ferrocene as a redox compound and 0.1 M Bu_4NClO_4 as a supporting electrolyte at a scan rate of 100 $mV\,s^{-1}$. A TiO_2 electrode or a SnO_2:F electrode was used as the working electrode, a Pt coil as the counter electrode, and an Ag^+/Ag electrode as the reference electrode. The surface morphology and the thickness of the TiO_2 thin film on the SnO_2:F substrate were observed with a Digital Instrument NanoScope Ⅲ A atomic force microscope (AFM).

Measurement of Photovoltaic Characteristics.　Figure 2 illustrates schematically the structure of the TiO_2/organic solid/ Au sandwich-type solar cell. The cell was fabricated as follows. First, the solid film of an organic insulator (Asahi Kagaku Lab., CR-30G-LL) was coated onto the TiO_2 electrode by screen-printing. Then, the PTh + MC blended solid film was coated onto the TiO_2 electrode by spin-coating. Finally, a gold electrode with a
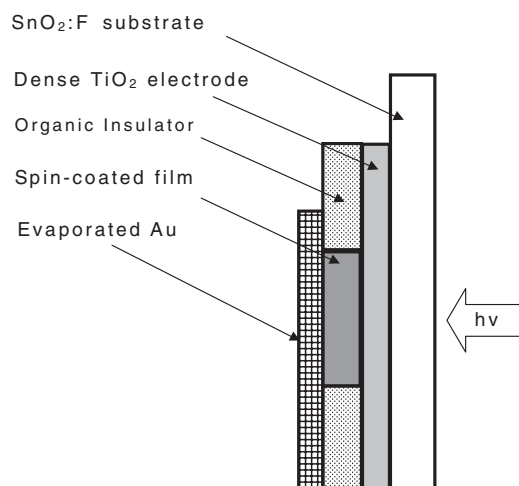
SnO₂:F substrate

Dense TiO₂ electrode

Organic Insulator

Spin-coated film

Evaporated Au

h ν

Fig. 2.　Schematic structure of solar cell.

thickness of about 25 nm was deposited onto the blended solid film by vacuum evaporation at 1×10^{-4} Torr. The photoactive area was confined to 0.25 cm^2. The thickness of the deposited Au film was monitored by an Ulvac CRTM-5000 oscillating quartz thickness controller, and the thickness d and mixing ratio R of the spin-coated organic solid film, which is defined by the molar ratio of MC to thiophene unit in PTh, were estimated from the amount and density of MC and PTh on the TiO_2 electrode. The amount was determined by a Hitachi U-3310 UV–visible spectrometer after dissolving the MC and PTh in chloroform. The densities of both MC and PTh were assumed to be 1.3 $g\,cm^{-3}$.[6]

The photocurrent-voltage characteristics were measured using a simulated solar light source of AM1.5–100 $mW\,cm^{-2}$ at a scan rate of 500 $mV\,min^{-1}$. The simulated solar light was obtained by a Kansai Kagakukikai XES-502S, and the light intensity was monitored by a SCIENTECH 365 power and energy meter.

The action spectra were measured at a scan rate of 60 $nm\,min^{-1}$. The light source consisted of a 750 W halogen tungsten lamp, and a Jasco CT-10 monochromator with a scanning controller SDM-25C was used. The light intensity was monitored by an Advantest TQ-8210 optical power meter with a silicon photocell. The photo-current was measured by an Advantest R-8240 electrometer and was recorded by a Yokogawa Denki 3057 portable recorder.

For the measurement of the electrical resistance of solid films in the dark and under AM1.5 illumination, an Au/organic solid/Au surface-type cell was employed. The interdigitated Au electrode, with a 150 μm gap and 207.7 mm long, was deposited on an alumina substrate before the spin-coating solid film was formed on it with a thickness of about 30 nm. The resistivity was estimated from the slope of the current-voltage line obtained by applying a ramp bias of 10 V and simultaneously measuring current.

The electric capacitance accumulated at the TiO_2/organic solid interface was measured in the dark as a function of the applied voltage by a low-frequency oscillographic method using a triangle wave.[6] A Hokuto Denko electrochemical analyzer, HAG-1512μ of the Hz-3000 series, was used for this measurement.

Results and Discussion

Characteristics of the TiO_2 Electrode.　Figure 3 shows cyclic voltammograms of the TiO_2 electrode and the SnO_2:F electrode in an acetonitrile solution containing ferrocene, Fc, as a redox compound. A pair of peaks for the redox reaction of Fc was observed for the SnO_2:F electrode, but the redox reaction was not observed for the TiO_2 electrode with about 100 nm
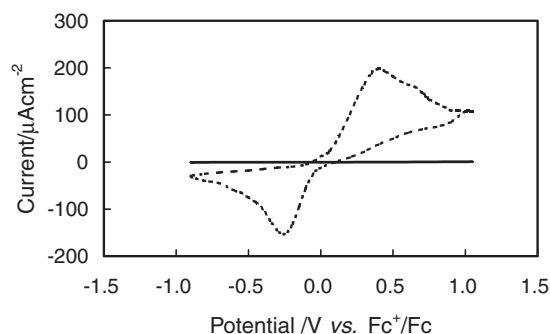
Fig. 3.　Cyclic voltammograms for the TiO_2 electrode (solid line) and SnO_2:F electrode (dotted line) in acetonitrile containing 1 mM ferrocene and 0.1 M Bt_4NClO_4 as supporting electrolyte. Scan rate was 100 $mV\,s^{-1}$.
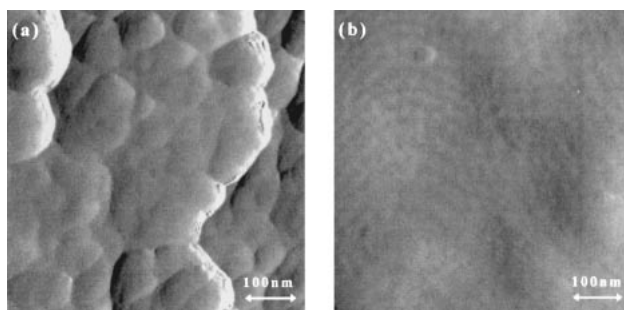
Fig. 4. AFM images of the SnO$_2$:F electrode (a) and the TiO$_2$ electrode (b).

thickness. When the TiO$_2$ electrode was soaked in 3×10^{-4} mol dm^{-3} MC1 ethanol solution for 24 h, MC1 was hardly adsorbed on the electrode despite of the carboxyl group in the MC1 molecule. On the other hand, many MC1 molecules were chemically adsorbed on a nano-porous TiO$_2$ electrode because of its carboxyl group (see Ref. 16). Figure 4 shows AFM images of the SnO$_2$:F electrode (a) as well as the TiO$_2$ electrode on the SnO$_2$:F substrate (b). The surface morphology of the TiO$_2$ electrode was much flatter than that of the SnO$_2$:F substrate. Further, the TiO$_2$ electrode on the SnO$_2$:F substrate was a non-porous film without cracks.

Photovoltaic Characteristics of the Solar Cells. We previously reported that a Schottky-barrier was formed at the interface between the low work function Al and solids with a p-type conductance of MC2 or PTh.[6] The bottom energy level of the conduction band of TiO$_2$ was 3.8–4.2 eV,[10,12,13] being nearly equal to the work function of Al. Therefore a p–n heterojunction or a Schottky barrier may be formed at the interface between TiO$_2$ and MC or PTh.

Figure 5 shows current-voltage characteristics of PTh (a), MC1 (b), and MC1 + PTh (c) solar cells under an illumination of AM1.5–100 mW cm^{-2}. The dark current-voltage curve for the pure MC1 and PTh cells did not exhibit a clear rectification property. On the other hand, the dark current-voltage curve for the MC1 + PTh blend cell exhibited some rectification behavior. Photovoltaic properties such as the short-circuit photocurrent, J_{sc}, open-circuit photovoltage, V_{oc}, fill factor, FF, and energy conversion efficiency, η under an illumination of AM1.5–100 mW cm^{-2} are summarized in Table 1. The values of $J_{sc} = 1.9$ μA cm^{-2}, $V_{oc} = 175$ mV, $FF = 20.2\%$, and $\eta = 7 \times 10^{-5}\%$ were obtained for the pure PTh solar cell. The values of $J_{sc} = 9.8$ μA cm^{-2}, $V_{oc} = 450$ mV, $FF = 28.3\%$, and
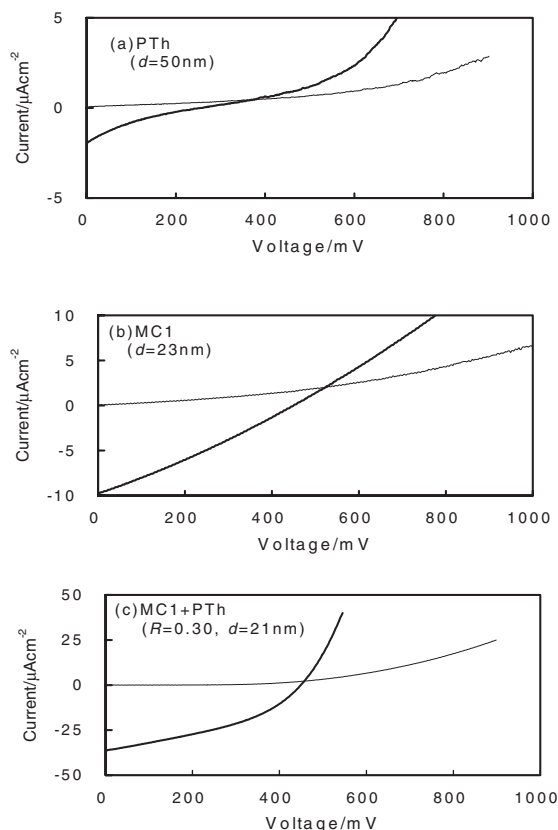

Fig. 5. Current-voltage characteristics of TiO$_2$/organic solid/Au sandwich-type solar cells with PTh (a), MC1 (b), and MC1 + PTh (c) under illumination of AM1.5–100 mW cm^{-2} (thick line) and in the dark (thin line). R is molar ratio of MC1 to thiophene unit in PTh, and d is the film thickness.

$\eta = 1.2 \times 10^{-3}\%$ were obtained for the pure MC1 solar cell. On the other hand, the higher values of $J_{sc} = 36.2$ μA cm^{-2}, $V_{oc} = 449$ mV, $FF = 39.5\%$, and $\eta = 6.4 \times 10^{-3}\%$ were obtained for the MC1 + PTh blended solar cell. The enhanced photovoltaic properties were also observed with the blend cell consisting of PTh and MC2, which does not have carboxyl group and long alkyl group. However, the η value for the MC2 + PTh blend cell was smaller than that for the MC1 + PTh blended cell, due to non-uniformity in the MC2 + PTh blended film. The reason for the enhanced performance in the blended cells will be discussed later.

Table 1. Performance of TiO$_2$/Organic Solid/Au Sandwich-Type Solar Cells under AM1.5–100 mW cm^{-2} Illumination

Organic solid	$R^{a)}$	$d^{b)}$ /nm	$J_{sc}{}^{c)}$ /μA cm^{-2}	$V_{oc}{}^{d)}$ /mV	$FF^{e)}$	$\eta^{f)}$ /%
PTh	0	50	1.9	175	20.2	7.0×10^{-5}
MC1	—	23	9.6	450	28.3	1.2×10^{-3}
MC1 + PTh	0.30	21	36.2	449	39.5	6.4×10^{-3}
MC2	—	38	3.0	40	24.5	3.0×10^{-5}
MC2 + PTh	0.31	56	25.3	442	26.2	2.9×10^{-3}

a) Molar ratio of merocyanine dye to thiophene unit in polythiophene. b) Film thickness. c) Short-circuit photocurrent density. d) Open-circuit photovoltage. e) Fill factor. f) Energy conversion efficiency.
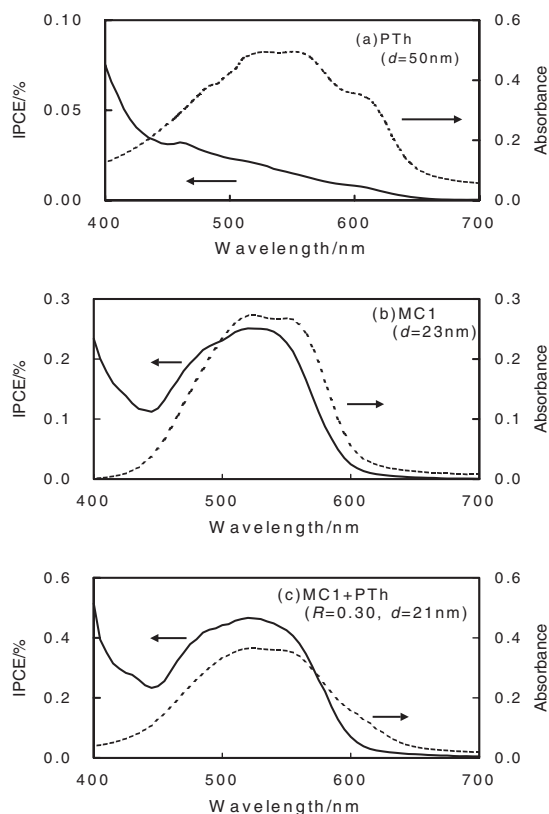
Fig. 6. Photocurrent action spectra of TiO$_2$/organic solid/
Au sandwich-type solar cells with PTh (a), MC1 (b), and
MC1 + PTh (c). *R* and *d* indicate the mixing molar ratio
and the film thickness, respectively, and *IPCE* is the inci-
dent photon to current conversion efficiency.

Figure 6 shows the short-circuit photocurrent action spectra
of the PTh (a), MC1 (b), and MC1 + PTh (c) solar cells for the
TiO$_2$ side illumination, and absorption spectra of their films on
a glass substrate. The direction of the photocurrent was from
the Au electrode to the TiO$_2$ electrode in the external circuit.
Incident photon to current conversion efficiency, *IPCE*, was
given by dividing the number of photo-generated electrons by
the incident photon number. The action spectra resembled
the absorption spectra. This indicates that the absorbed photons
in the organic solid were employed for the photocurrent gener-
ation, and that the photoactive site was at the TiO$_2$/organic sol-
id interface. The *IPCE* value for the MC1 + PTh blended cell
was large compared to that for the pure MC1 or PTh solar cell.
This indicates that the efficiency of the photocharge separation
for the blended cell increased, increasing the η value.

Figure 7 shows the dependence of the short-circuit photocur-
rent, open-circuit photovoltage, fill factor, and energy conver-
sion efficiency in the MC1 + PTh blend cell on the thickness
of the blended film. The J_{sc} and *FF* values increased up to a
thickness of about 20 nm, the V_{oc} value increased up to about
10 nm, and the η value increased up to about 20 nm. We cannot
explain the inconsistency between the thickness dependence of
J_{sc} and V_{oc}. For an electric field formed at the TiO$_2$/organic
solid interface, we will discuss later.

Only a mono-layer of MC1 has been chemically adsorbed on
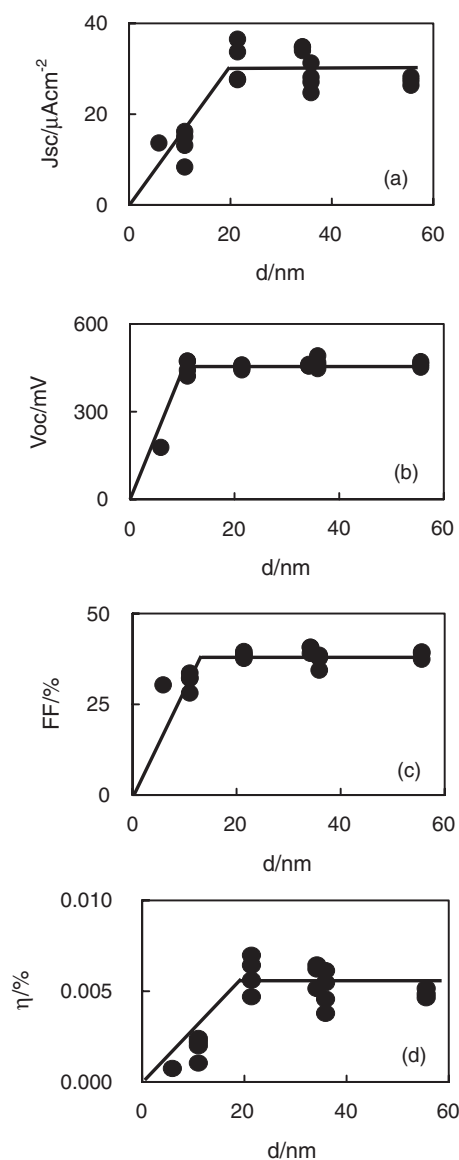a TiO$_2$ nano-porous electrode in the dye-sensitized solar cells,

Fig. 7. Film thickness dependence of short-circuit photocur-
rent J_{sc} (a), open-circuit photovoltage V_{oc} (b), fill factor *FF*
(c) and energy conversion efficiency η (d) under illumina-
tion of AM1.5–100 mW cm^{-2} for the MC1 + PTh
($R = 0.3$) blended solar cell.

so-called Grätzel cell.[16] On the other hand, since we used a
dense and non-porous TiO$_2$ electrode on which the MC1 mole-
cules with a carboxyl group hardly adsorbed, the photocurrent
generation mechanism for the blended cells may be different
from that of Grätzel cells.

Effect of Photoinduced Charge Transfer. We previously
reported that when a photoinduced hole-transfer occurred from
the HOMO level of MC2 to the valence band of PTh in an Al/
MC2 + PTh Schottky-barrier cell, the photovoltaic properties
were improved.[6] Since the HOMO levels of MC1 and MC2
are nearly equal, based on cyclic voltammetry in dichloro-
methane containing MC1 or MC2, photoexcited holes in
MC1 can be injected in to the valence band of PTh. The photo-
produced holes in PTh were transported to the Au electrode by
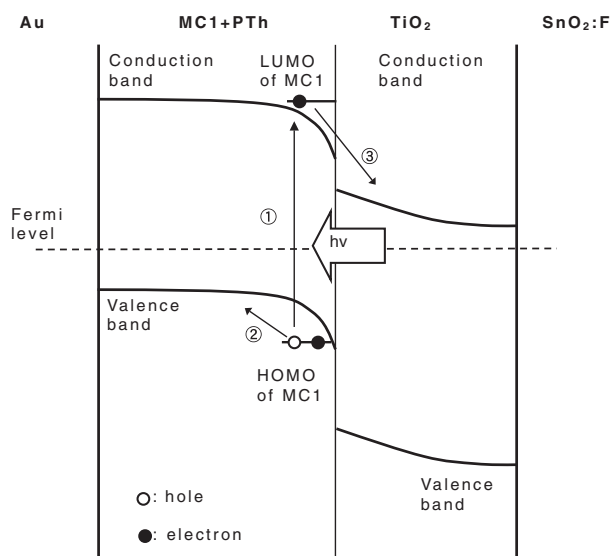the electric field formed at the interface of TiO$_2$ and the blended

Fig. 8. Schematic energy diagram for TiO$_2$/MC1 + PTh/ Au sandwich-type solar cell. See the text for the explanation of the sequence numbers ①, ②, and ③.

film, on the other hand, the photoproduced electrons arrived at the TiO$_2$ electrode. This proposal of the photocurrent generation mechanism is shown in Fig. 8. First, MC1 in the blended solid is excited (process ①). Second, the charge transfer occurs between the excited MC1 and the ground-state PTh (process ②). Finally, the resulting holes and electrons are transported to the Au and TiO$_2$ electrodes, respectively (process ③). When discrete pairs of electrons and holes are produced by photo-induced hole-transfer from MC1 to PTh, the coulombic force between the electron and the hole is much smaller than that in the excited MC1 molecule because of the large distance. These results in photocharge separation in the blended solar cell proceeding more easily by the electric field formed at the interface of TiO$_2$ and the organic solid.

Influence of the Series Electrical Resistance of the Solar Cell. The magnitude of the series electrical resistance of the solar cell is generally an important factor for determining the photovoltaic properties. The value estimated from the cur-

rent-voltage characteristics in Fig. 5 was 2.6×10^4 $\Omega \, cm^{-2}$ for the PTh cell (a), 1.8×10^4 $\Omega \, cm^{-2}$ for the MC1 cell (b), and 1.0×10^4 $\Omega \, cm^{-2}$ for the MC1 + PTh blend cell (c) under an illumination of AM1.5–100 mW cm^{-2}, as summarized in Table 2. The order of the magnitude was MC1 + PTh < MC1 < PTh, the solar cell with a smaller series resistance indicating a higher performance.

The specific resistivity of organic solid films is summarized in Table 3. Under illumination, the resistivity of MC1 was over 10^9 $\Omega \, cm$, and that of PTh and MC1 + PTh was 9.3×10^5 $\Omega \, cm$ and 1.3×10^7 $\Omega \, cm$, respectively. Since the order of the specific resistivities was MC1 > MC1 + PTh > PTh, it can be said that the photovoltaic properties are not necessary influenced by this factor.

Electric Field Formed at the TiO$_2$/Organic Solid Interface. The electric capacitance, C, at the TiO$_2$/organic solid interface was measured in the dark as a function of the applied voltage by a low-frequency oscillographic method using a triangle wave.[6] When the applied ramp bias increases, the observed current, J_+, is the sum of discharging and ohmic currents:

$$J_+ = C(dV/dt) + V/rr, \tag{1}$$

where V, dV/dt, and rr are the applied voltage, the scan rate of the applied voltage, and the resistance, respectively. When the voltage decreases, the current, J_-, is the sum of charging and ohmic currents,

$$J_- = -C(dV/dt) + V/rr. \tag{2}$$

Combining the above two equations, the capacitance is expressed:

$$C = (J_+ - J_-)/2(dV/dt). \tag{3}$$

Further, because dV/dt is equal to $4V_0 f$, where V_0 is the amplitude of the applied voltage and f is the frequency of the ramp bias, the capacitance can be expressed as:

$$C = (J_+ - J_-)/8V_0 f. \tag{4}$$

When the current density is used for J_+ and J_-, C represents the capacitance per unit area. The insets of Fig. 9 show the current-voltage curve under the application of a ramp bias between

Table 2. Series Resistance of TiO$_2$/Organic Solid/Au Sandwich-Type Solar Cells

Organic solid	R	d/nm	R_{int}[a]/$\Omega \, cm^{-2}$	
			in dark	under illumination[b]
PTh	0	70	6.1×10^5	2.6×10^4
MC1	—	23	2.3×10^5	1.8×10^4
MC1 + PTh	0.30	56	3.0×10^5	1.0×10^4

a) Series resistance. b) Under AM1.5–100 mW cm^{-2}.

Table 3. Specific Resistivity of Organic Solid

Organic solid	R	d/nm	ρ[a]/$\Omega \, cm$	
			in dark	under illumination[b]
PTh	0	43	1.4×10^6	9.3×10^5
MC1 + PTh	0.30	42	2.5×10^7	1.3×10^7

a) Specific resistivity. b) Under AM1.5–100 mW cm^{-2}.
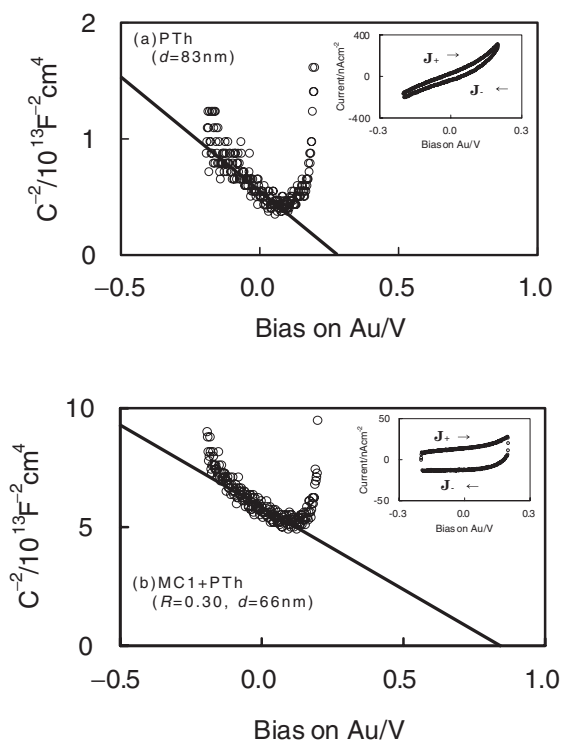
Fig. 9. Mott–Schottky plots of TiO$_2$/organic solid/Au sandwich-type solar cells with PTh (a) and MC1 + PTh (b). Insets show dark current-voltage curves at the frequencies of 94 mHz (a), and 125 mHz (b). The arrows in the insets show the direction of the potential sweep. See text for the definition of J_+ and J_-.

−0.2 and +0.2 V ($V_0 = 0.2$ V).

On the assumption that a p–n hetero-junction is formed at the TiO$_2$/organic interface, Anderson's model was applied to analyze the electric profile at the interface, being employed for a p–n hetero-junction organic cell by Chamberlain.[17] In this model, the capacitance is expressed as a function of the bias:

$$C^{-2} = (\varepsilon_n N_p + \varepsilon_p N_n)^2 (V_b - V)$$
$$/[(\varepsilon_n N_n + \varepsilon_p N_p)\varepsilon_n \varepsilon_p \varepsilon_0 q N_n N_p A^2], \quad (5)$$

where ε_n is the relative dielectric constant of an n-type semiconductor, ε_p is the relative dielectric constant of a p-type semiconductor, ε_0 is the vacuum permitivity, q is the electron charge, N_n is the density of the ionized carrier in the n-type semiconductor, N_p is the ionized carrier density in the p-type semiconductor, V_b is the built-in potential of the p–n hetero-junction, and A is the active area. The subscripts n and p represent TiO$_2$ as the n-type semiconductor and the organic solid as the p-type semiconductor, respectively.

As shown in Fig. 9(a), the plot of C^{-2} against V, a so-called Mott–Schottky plot, for the pure PTh cell gave a straight line in the range between −0.15 and +0.05 V. We obtained $V_b = 0.25$ V. When $N_p = 6.0 \times 10^{17}$ cm^{-3},[6] $\varepsilon_p = 4$,[6] and $\varepsilon_n = 48$[18] were used, the value of 1.7×10^{17} cm^{-3} was obtained for N_n. Following equations 6 and 7, we obtained $W_p = 12$ nm, $W_n = 51$ nm, where W_p and W_n represent the widths of the depletion layers in the p-type PTh and the n-type TiO$_2$ under short-circuit conditions, respectively:

$$W_p = [2N_n \varepsilon_n \varepsilon_p V_b / [qN_p(\varepsilon_n N_p + \varepsilon_p N_n)]]^{1/2}, \quad (6)$$

$$W_n = [2N_p \varepsilon_n \varepsilon_p V_b / [qN_n(\varepsilon_n N_p + \varepsilon_p N_n)]]^{1/2}. \quad (7)$$

Further, from Eqs. 8 and 9, we obtained $V_{bp} = 0.184$ V and $V_{bn} = 0.066$ V, where V_{bp} and V_{bn} represent the built-in potentials in the p-type PTh and in the n-type TiO$_2$ under short-circuit condition, respectively.

$$V_{bp}/V_{bn} = \varepsilon_n N_n / (\varepsilon_p N_p), \quad (8)$$

$$V_b = V_{bp} + V_{bn}. \quad (9)$$

Since the Mott–Schottky plot for the MC1 + PTh blend cell gave a straight line between −0.15 and +0.10 V, as shown in Fig. 9(b), we obtained $V_b = 0.620$ V and $N_p = 6.9 \times 10^{17}$ cm^{-3} from Eq. 5, and further $W_p = 20$ nm, $W_n = 80$ nm, $V_{bp} = 0.613$ V, and $V_{bn} = 0.207$ V from Eqs. 6, 7, 8, and 9, respectively. These parameters are summarized in Table 4. The W_p value of the MC1 + PTh blend cell was nearly equal to the region of the photocurrent generation estimated from the thickness dependence of the photovoltaic properties in Fig. 7.

Under short-circuit conditions, the potential gradient V_{bp}/W_p on the PTh side of the TiO$_2$/PTh interface was 3.9×10^5 V cm^{-1}, and V_{bn}/W_n on the TiO$_2$ side was 3×10^4 V cm^{-1}. Further, for the MC1 + PTh blend cell, the values of 7.7×10^5 V cm^{-1} and 6×10^4 V cm^{-1} were obtained for V_{bp}/W_p and the V_{bn}/W_n, respectively. Since the electric field on the organic solid side of both cells was much larger than that on the TiO$_2$ side, this type of solar cell may be regarded as a TiO$_2$/organic solid Schottky barrier cell rather than a p–n hetero-junction cell.

Since the value of the electric field on the organic solid side of both solar cells, MC1 + PTh > PTh, agreed with that of the energy conversion efficiency, η, to within on order of magnitude, there exists the opportunity to improve the photovoltaic properties.

Conclusions

In the TiO$_2$/organic solid/Au sandwich-type cells, the photovoltaic properties were much better for the MC1 + PTh blended cell than for the pure PTh cell. This is because an effective photoinduced hole-transfer occurred from the excited of

Table 4. Ionized Carrier Density N in the Organic Solid, Built-in Potential V_b in TiO$_2$/Organic Solid/Au Sandwich-Type Solar Cells, and Depletion Layer Width W at the TiO$_2$/Organic Solid Interface under Short-Circuit Condition

	R	d /nm	N_p /10^{17} cm^{-3}	N_n /10^{17} cm^{-3}	W_p /nm	W_n /nm	V_{bp} /mV	V_{bn} /mV	V_{bp}/W_p /10^5 V cm^{-1}	V_{bn}/W_n /10^5 V cm^{-1}
PTh	0	83	6.0[a]	1.7	12	51	184	66	3.9	0.3
MC1 + PTh	0.30	66	6.9	1.7	20	80	613	207	7.7	0.6

a) From Ref. 6.

MC1 to the ground-state of PTh, accelerating the photocharge separation in the depletion layer formed at the interface of TiO_2 and MC1 + PTh. The depletion layer existed in the narrow region of about 20 nm on the organic solid side, and the electric field was about 8×10^5 V cm^{-1}. That is, the blended solar cell in this work is not a so-called Grätzel cell being sensitized by mono-layer dyes chemically adsorbed on to a TiO_2 electrode, but rather the enhanced photovoltaic properties are attributable to the dye-sensitization of the regioregular polythiophene.

We think further modifications of the conjugated polymer, sensitizer, and TiO_2 electrode would increase the electric filed of the depletion layer or/and the thickness of the depletion layer. In fact, we recently obtained the photovoltaic properties of $J_{sc} = 814$ μA cm^{-2}, $V_{oc} = 737$ mV, $FF = 56\%$, and $\eta = 0.33\%$ under AM1.5–100 mW cm^{-2} illumination in a new-type TiO_2/MC1 + PTh blend solar cell fabricated with the TiO_2 electrode prepared by a different method. This will be reported elsewhere in detail.

References

1 C. W. Tang, *Appl. Phys. Lett.*, **48**, 183 (1986).

2 M. Granstrom, K. Petritsch, A. C. Arias, A. Lux, M. R. Andersson, and R. H. Friend, *Nature*, **395**, 257 (1998).

3 C. J. Brbec, S. E. Shaheen, C. Winder, and N. S. Sariciftci, *Appl. Phys. Lett.*, **80**, 1288 (2002).

4 K. Takahashi, T. Goda, T. Yamaguchi, and T. Komura, *J. Phys. Chem. B*, **103**, 4868 (1999).

5 K. Takahashi, T. Iwanaga, T. Yamaguchi, T. Komura, and K. Murata, *Synth. Met.*, **123**, 91 (2001).

6 K. Takahashi, K. Tsuji, K. Imoto, T. Yamaguchi, T. Komura, and K. Murata, *Synth. Met.*, **130**, 177 (2002).

7 K. Takahashi, M. Asano, K. Imoto, T. Yamaguchi, T. Komura, J. Nakamura, and K. Murata, *J. Phys. Chem. B*, **107**, 1646 (2003).

8 K. Takahashi, I. Nakajima, K. Imoto, T. Yamaguchi, T. Komura, J. Nakamura, and K. Murata, *Sol. Energy Mater. Sol. Cells*, **76**, 115 (2003).

9 K. Murata, S. Ito, K. Takahashi, and B. M. Holfman, *Appl. Phys. Lett.*, **71**, 674 (1997).

10 T. J. Savenije, J. M. Warman, and A. Goossens, *Chem. Phys. Lett.*, **24**, 148 (1998).

11 W. U. Huynh, J. J. Dittmerm, and A. P. Alevisatos, *Science*, **295**, 2425 (2002).

12 A. C. Arango, L. R. Johnson, V. N. Bliznyuk, Z. Schlesinger, S. A. Carter, and H. H. Hörhold, *Adv. Mater.*, **12**, 1689 (2000).

13 Q. Fan, B. McQuillin, D. D. C. Bradley, S. Whitelegg, and A. B. Seddon, *Chem. Phys. Lett.*, **26**, 325 (2001).

14 C. D. Grant, A. M. Schwartzberg, G. P. Smestad, J. Kowalik, L. M. Tolbert, and Z. Zhang, *Synth. Met.*, **132**, 197 (2003).

15 P. A. van Hal, M. Wienk, J. M. Kroon, W. J. H. Verhees, L. H. Slooff, W. J. H. van Gennip, P. Jonkheijm, and R. A. J. Janssen, *Adv. Mater.*, **15**, 118 (2003).

16 K. Sayama, S. Tsukagoshi, K. Hara, Y. Ohga, A. Shinpou, Y. Abe, S. Suga, and H. Arakawa, *J. Phys. Chem. B*, **106**, 1363 (2002).

17 G. A. Chamberlain, *Mol. Cryst. Liq. Cryst.*, **93**, 369 (1983).

18 M. Kiyono, "Sankatitan," Gihoudou, Tokyo (1991), p. 52.